*Geophys. J. Int.* (1999) **138,** 747–756

# Seismic waves converted from velocity gradient anomalies in the Earth's upper mantle

M. G. Bostock

*Department of Earth and Ocean Sciences, University of British Columbia, Vancouver, British Columbia, Canada,* V6T 1Z4. *E-mail: bostock@geop.ubc.ca*

Accepted 1999 April 19. Received 1999 April 11; in original form 1998 September 24

## SUMMARY

Modelling of elastic wave propagation in 1-D structures is frequently performed using reflectivity techniques in which the Earth's velocity profile is approximated by stacks of homogeneous layers. The complete reflection/transmission (R/T) response of a zone with arbitrary 1-D depth variation (including both gradients and discontinuities in material properties) can, however, be calculated using invariant embedding techniques. Results from earlier studies are here extended to derive exact expressions for R/T matrices in arbitrary, 1-D anisotropic media using a form of Born approximation valid for thin scatterers and which does not assume small perturbations in material properties. The R/T matrices are solutions to a system of non-linear, ordinary differential equations of Ricatti type and may be manipulated using standard R/T matrix algebra. In an equivalent description, the wavefield within the heterogeneous zone is considered in terms of depth-dependent contributions from up- and downgoing waves propagating within the embedding reference medium. This leads to efficient calculation of the internal wavefield using R/T matrices of the heterogeneous stratification and portions thereof at minor additional expense. Mode conversion of teleseismic *P* and *S* phases from velocity gradients is examined by way of examples and comparison with three-component data from broad-band stations of the Yellowknife seismic array. The frequency dependence of such wave interactions depends on the differences in vertical slowness between incident and scattered modes. It is shown that significant energy is converted from transition zones with extent $L < \lambda_P/2$, a broader interval than will generally produce intramode reflections. A layer structure identified from *Ps* conversions near 75 km depth below the Slave craton is shown to be compatible with a $\sim$10 km thick gradient zone in which anisotropy increases from ambient levels to $\delta V_p = \pm 5$ per cent, $\delta V_s = \pm 2.5$ per cent at a discontinuous upper boundary. This characterization supports a previous interpretation as the upper strata of a former oceanic plate juxtaposed against overriding lithosphere during an ancient episode of shallow subduction.

**Key words:** body waves, lithosphere, mantle discontinuities, mode coupling, seismic wave propagation.

## INTRODUCTION

Inferences on geodynamic processes drawn from seismological characterization of Earth structure often rely on an accurate assessment of the scales at which elastic properties vary. This observation has provided strong motivation for recent progress in detailed tomographic imaging of Earth structure from increasingly comprehensive seismological data sets (e.g. Grand 1994; van der Hilst *et al.* 1997). However, accurate reconstruction of material property gradients in tomographic studies is compromised by the need for model regularization, which results in image distortion, in particular the attenuation of high-wavenumber components. An alternative approach to the characterization of spatial gradients in velocity is to monitor the frequency dependence of waves scattered from rapid structural variations (what constitutes rapid is necessarily a function of frequency). This approach has proved useful in documenting so-called discontinuities within the Earth's crust and mantle that are more properly represented as transition intervals of finite width (Richards 1972; Benz & Vidale 1993; Petersen *et al.* 1993).

The subject of this paper is the description of body waves scattered from 1-D variations in velocity and density. Previous work on this subject has dealt largely with asymptotic

treatments (Richards 1972; Chapman 1974; Richards & Frasier 1976; Woodhouse 1978; Kennett & Illingworth 1981); however, we shall adopt an approach which allows us to extract the broad-band reflection and transmission response of the heterogeneity using the principles of invariant embedding (Ursin 1983; Bellman & Vasudevan 1986; McCoy & Frazer 1986; Tromp & Snieder 1989). Exact expressions are derived for the reflection and transmission operators in arbitrary, anisotropic, plane-stratified media in terms of material property perturbations from a reference structure. The derivation follows the general approach of Tromp & Snieder (1989) but starts from the equations of motion and documents several important modifications to that work, specifically (i) the use of a thin-scatterer approximation (versus the conventional Born approximation), which renders the treatment exact, (ii) a modification to the boundary conditions on transmission as required by the perturbation approach, and (iii) an extension of the treatment to allow for description of the wavefield within the zone of heterogeneity. Several examples are presented to demonstrate application of the theory to mode conversion of teleseismic waves in the Earth's upper mantle. In particular, comparison of synthetic seismograms with the observed teleseismic impulse response at Yellowknife, Northwest Territories, places further constraints on the nature of lithospheric mantle layering recently documented below the Slave province (Bostock 1998).

## THEORETICAL DEVELOPMENT

We begin with the elastic wave equation for a homogeneous, anisotropic medium in the absence of sources,

$$c_{ijkl}u_{k,lj} - \rho \frac{\partial^2 u_i}{\partial t^2} = 0 . \tag{1}$$

This expression may be Fourier transformed with respect to the two transverse coordinates $(x_1, x_2)$ $[=(x, y)]$ to yield an ordinary differential equation describing the displacement $u_j$ of monochromatic plane waves as

$$L_{ij}u_j = 0 , \tag{2}$$

where the differential operator $L_{ij}$ is defined by

$$L_{ij} = (\mathbf{C}_{33})_{ij} \frac{\mathrm{d}^2}{\mathrm{d}z^2} - \mathrm{i}\omega p_\alpha (\mathbf{C}_{3\alpha} + \mathbf{C}_{\alpha 3})_{ij} \frac{\mathrm{d}}{\mathrm{d}z} + \omega^2(\rho\delta_{ij} - p_\alpha p_\gamma (\mathbf{C}_{\alpha\gamma})_{ij}) . \tag{3}$$

Here, $\rho$ is density, $\omega$ is radial frequency, $p_\alpha$ is the phase slowness in the $\alpha$-direction, and we have adopted a notation similar to Woodhouse (1974) to represent the anisotropic elastic tensor $c_{ijkl}$ by matrices $\mathbf{C}_{ij}$ as $(C_{ij})_{kl} = c_{kilj}$. Roman and Greek subscripts denote vectors in 3 and 2 horizontal dimensions, respectively, with the summation convention for repeated subscripts holding in both instances. Eq. (2) also applies to individual subdomains of a piecewise homogeneous medium and it is our intention to use it in the analysis of scattering from a thin homogeneous horizontal slab of material on $[z_a, z_b]$ whose properties differ from that of an external, otherwise homogeneous reference medium (see Fig. 1). It is convenient therefore to define reference and perturbation operators $L^0_{ij}$, $\Delta L_{ij}$ such that $L_{ij} = L^0_{ij} + \Delta L_{ij}$ and $\Delta L_{ij}$ vanishes outside the slab. We will further divide the displacement into incident and scattered components, $u_i = u^0_i + \Delta u_i$, where $L^0_{ij}u^0_j = 0$. This construction leads to the derivation of an equation

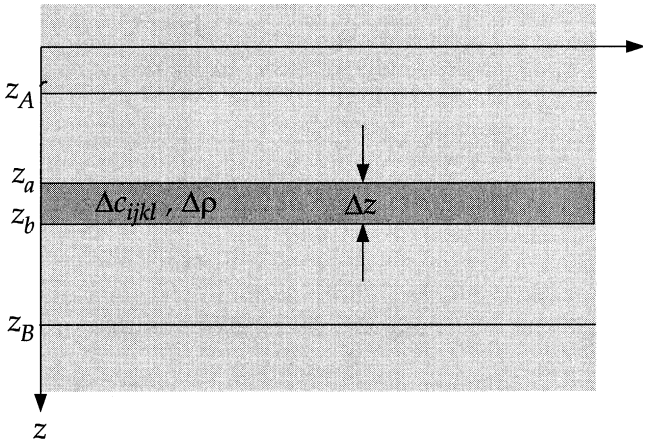


**Figure 1.** Derivation of the R/T response for a zone of arbitrary 1-D heterogeneity relies upon an exact expression for the response of a vanishingly thin ($\Delta z \to 0$) slab of material exhibiting arbitrary departures in physical properties ($\Delta c_{ijkl}$, $\Delta\rho$) from the embedding reference medium.

$$L^0_{ij}\Delta u_j = -\Delta L_{ij}u_j , \tag{4}$$

where the scattered wave can be seen to arise from the material perturbation. The form of differential equation in (2) requires that we further consider the adjoint operator $L^{0\dagger}_{ij}$,

$$L^{0\dagger}_{ij} = (\mathbf{C}^0_{33})_{ij} \frac{\mathrm{d}^2}{\mathrm{d}z^2} + \mathrm{i}\omega p_\alpha (\mathbf{C}^0_{3\alpha} + \mathbf{C}^0_{\alpha 3})_{ij} \frac{\mathrm{d}}{\mathrm{d}z} + \omega^2(\rho^0\delta_{ij} - p_\alpha p_\gamma (\mathbf{C}^0_{\alpha\gamma})_{ij}) , \tag{5}$$

and associated Green's function $G^\dagger_{in}(z, z')$, which solves

$$L^{0\dagger}_{ij} G^\dagger_{jn}(z, z') = -\delta_{in}\delta(z - z') . \tag{6}$$

Note that $G^\dagger_{in}$ is related to the Green's function $G_{in}(z, z')$ for $L^0_{ij}$ as $G^\dagger_{in}(z, z') = G_{ni}(z', z)$. Although the formulation allows for other choices it will prove expedient to adopt an isotropic reference medium for which a simple analytic form of the 1-D Green's tensor is available (see e.g. Tromp & Snieder 1989):

$$G_{in}(z, z') = \begin{cases} \displaystyle\sum_{r=1}^{3} \frac{\mathrm{i}\,\mathrm{e}^{-\mathrm{i}\omega q^r z}\,\mathrm{e}^{\mathrm{i}\omega q^r z'}}{2\omega\rho^0 (v^r)^2 q^r} \hat{s}^r_i \check{s}^r_n & z < z' \\ \displaystyle\sum_{r=1}^{3} \frac{\mathrm{i}\,\mathrm{e}^{\mathrm{i}\omega q^r z}\,\mathrm{e}^{-\mathrm{i}\omega q^r z'}}{2\omega\rho^0 (v^r)^2 q^r} \check{s}^r_i \check{s}^r_n & z > z' \end{cases} . \tag{7}$$

The index $r = 1, 2, 3$ identifies $P$, $SV$ and $SH$ waves, $v^r$ and $q^r = p^r_3 = \sqrt{(v^r)^{-2} - p_\alpha p_\alpha}$ are the velocity and the vertical slowness for mode $r$, and $\hat{s}^r_i$, $\check{s}^r_i$ are the polarization vectors of up- and downgoing modes, respectively, normalized to unit displacement. Specifically, we set

$$\begin{aligned} \check{s}^{(1)}_i &= v^{(1)}[p_1, p_2, q^{(1)}]^{\mathrm{T}} , \\ \check{s}^{(2)}_i &= v^{(2)}q^{(2)}[p_1, p_2, -p_\alpha p_\alpha / q^{(2)}]^{\mathrm{T}} / \sqrt{p_\alpha p_\alpha} , \\ \check{s}^{(3)}_i &= [-p_2, p_1, 0]^{\mathrm{T}} / \sqrt{p_\alpha p_\alpha} \end{aligned} \tag{8}$$

for downgoing modes, and

$$\hat{s}_i^{(1)} = v^{(1)}[p_1, p_2, -q^{(1)}]^{\mathrm{T}},$$

$$\hat{s}_i^{(2)} = v^{(2)} q^{(2)}[p_1, p_2, p_\alpha p_\alpha / q^{(2)}]^{\mathrm{T}} / \sqrt{p_\alpha p_\alpha}, \tag{9}$$

$$\hat{s}_i^{(3)} = [-p_2, p_1, 0]^{\mathrm{T}} / \sqrt{p_\alpha p_\alpha}$$

for upgoing modes.

The derivation proceeds by contracting (6) with $\Delta u_i$ and (4) with $G^{\dagger}_{in}(z, z')$, subtracting, and integrating over an arbitrary depth interval $[z_A, z_B]$ encompassing the thin slab. This allows the scattered field to be expressed in the form of a Lippman–Schwinger integral equation,

$$\Delta u_n(z') = \int_{z_a}^{z_b} \mathrm{d}z - \frac{\mathrm{d}G^{\dagger}_{in}}{\mathrm{d}z} (\Delta \mathbf{C}_{33})_{ij} \frac{\mathrm{d}u_j}{\mathrm{d}z} + \mathrm{i}\omega p_\alpha G^{\dagger}_{in} (\Delta \mathbf{C}_{\alpha 3})_{ij} \frac{\mathrm{d}u_j}{\mathrm{d}z}$$

$$- \mathrm{i}\omega p_\alpha \frac{\mathrm{d}G^{\dagger}_{in}}{\mathrm{d}z} (\Delta \mathbf{C}_{3\alpha})_{ij} u_j + G^{\dagger}_{in} \omega^2 (\Delta\rho \delta_{ij} - p_\alpha p_\gamma (\Delta \mathbf{C}_{\alpha\gamma})_{ij}) u_j . \tag{10}$$

In deriving (10) a number of terms have been evaluated through integration by parts over piecewise homogenous domains, and we have made use of the boundary conditions of continuous displacement and traction which, in the latter case, may be written as e.g.

$$\left[ (\Delta \mathbf{C}_{33})_{ij} \frac{\mathrm{d}u_j}{\mathrm{d}z} + \mathrm{i}\omega p_\alpha (\Delta \mathbf{C}_{3\alpha})_{ij} u_j \right]_{z_a^-}^{z_a^+} = \left[ -(\mathbf{C}^0_{33})_{ij} \frac{\mathrm{d}\Delta u_j}{\mathrm{d}z} \right]_{z_a^-}^{z_a^+}, \tag{11}$$

with a similar relation holding at $z_b$.

We seek an approximation to eq. (10) which becomes exact as the thickness of the slab $\Delta z (= z_b - z_a)$ goes to zero. This cannot be achieved by way of the conventional Born approximation (i.e. setting $u_i \approx u_i^0$) since although $u_i$ is continuous across the slab boundaries, its derivatives, in general, are not (e.g. Herrera & Mal 1965). To develop a 'thin scatterer' approximation, the relevant quantities are recast in the $6 \times 6$ Voigt notation. The constitutive relation becomes

$$\tau_p = c_{pq} e_q, \quad p, q = 1, 6, \tag{12}$$

where the elastic tensor is

$$c_{pq} \equiv c_{ijkl}, \quad p, q = 1, 6, \quad i, j, k, l = 1, 3, \tag{13}$$

and indices correspond as

| $ij/kl$ | 11 | 22 | 33 | 23, 32 | 31, 13 | 12, 21 |
|---|---|---|---|---|---|---|
| $p/q$ | 1 | 2 | 3 | 4 | 5 | 6 |

. (14)

Boundary conditions dictate that components of stress normal to the slab (i.e. $\tau_3$, $\tau_4$, $\tau_5$) and components of strain parallel to the slab (i.e. $e_1$, $e_2$, $e_6$) are continuous across the slab boundaries at $z_a$ and $z_b$. It is therefore convenient to define

$$\mathsf{A} = \begin{pmatrix} 1 & 0 & 0 & 0 & 0 & 0 \\ 0 & 1 & 0 & 0 & 0 & 0 \\ c_{31} & c_{32} & c_{33} & c_{34} & c_{35} & c_{36} \\ c_{41} & c_{42} & c_{43} & c_{44} & c_{45} & c_{46} \\ c_{51} & c_{52} & c_{53} & c_{54} & c_{55} & c_{56} \\ 0 & 0 & 0 & 0 & 0 & 1 \end{pmatrix}, \tag{15}$$

where $\mathsf{A}$ is equivalent to the elasticity matrix $\mathsf{C}$ (that is $c_{pq}$) on rows 3, 4, 5 and is unit diagonal on rows 1, 2, 6 (note the use of different fonts to distinguish the $6 \times 6$ Voigt matrices from the $3 \times 3$ $\mathbf{C}_{ij}$ matrices). This construction leads to a relation between the displacement field immediately within the slab $u_i^-$ and that immediately outside $u_i^+$ by way of an effective elastic tensor $\Delta \tilde{c}_{ijkl}$:

$$\Delta c_{ijkl} u^-_{k,l} = \Delta \tilde{c}_{ijkl} u^+_{k,l}, \tag{16}$$

where $\Delta \tilde{c}_{ijkl}$ is defined in Voigt notation by

$$\Delta \widetilde{\mathsf{C}} = \Delta \mathsf{C} (\mathsf{A}^-)^{-1} (\mathsf{A}^+). \tag{17}$$

Here, $\Delta \mathsf{C}$ is the elastic perturbation tensor $\Delta c_{ijkl}$ in Voigt notation, and superscripts $^-$, $^+$ again refer to properties immediately inside and outside the slab, respectively. When applied to isotropic media, $\Delta \widetilde{\mathsf{C}}$ reduces to the forms given by Hudson (1977) (see also Kennett 1984), and possesses the general structure of an elastic tensor describing hexagonal anisotropy with a vertical symmetry axis. This lends some insight into how a finely layered, horizontal sequence of isotropic beds with alternating high and low velocities comes to exhibit a macroscopic transverse isotropy or 'long-wave' anisotropy (Backus 1962).

Derivation of the thin-scatterer Born approximation involves simply recasting the effective elastic modulus $\Delta \widetilde{\mathsf{C}}$ in the Woodhouse (1974) notation (i.e. $\Delta \widetilde{\mathbf{C}}_{ij}$), invoking the reciprocal relation $G^{\dagger}_{in}(z, z') = G_{ni}(z', z)$, setting $u_i^+ \approx u_i^0$, and substituting (16) into (10) as follows:

$$\Delta u_n(z') \approx \Delta z \left( - \frac{\mathrm{d}G_{ni}(z', z)}{\mathrm{d}z} (\Delta \widetilde{\mathbf{C}}_{33})_{ij} \frac{\mathrm{d}u_j^0}{\mathrm{d}z} \right.$$

$$+ \mathrm{i}\omega p_\alpha G_{ni}(z', z) (\Delta \widetilde{\mathbf{C}}_{\alpha 3})_{ij} \frac{\mathrm{d}u_j^0}{\mathrm{d}z}$$

$$- \mathrm{i}\omega p_\alpha \frac{\mathrm{d}G_{ni}(z', z)}{\mathrm{d}z} (\Delta \widetilde{\mathbf{C}}_{3\alpha})_{ij} u_j^0$$

$$\left. + G_{ni}(z', z) \omega^2 (\rho^0 \delta_{ij} - p_\alpha p_\gamma (\Delta \widetilde{\mathbf{C}}_{\alpha\gamma})_{ij}) u_j^0 \right), \tag{18}$$

which is correct to first order in slab thickness $\Delta z$.

To gain insight into the scattering properties of the slab, consider as an example an upgoing incident wave represented by

$$u_i^0 = \sum_{r=1}^{3} \hat{a}^r \, \mathrm{e}^{-\mathrm{i}\omega q^r z} \hat{s}_i^r, \tag{19}$$

where $\hat{a}^r$ is a wave vector which controls the contributions from individual modes. This will produce upward transmitted and downward reflected waves which are accordingly expanded as

$$\Delta u_i = \sum_{r=1}^{3} \hat{b}^r \, \mathrm{e}^{-\mathrm{i}\omega q^r z} \hat{s}_i^r, \quad z < z_a \tag{20}$$

and

$$\Delta u_i = \sum_{r=1}^{3} \check{b}^r \, \mathrm{e}^{\mathrm{i}\omega q^r z} \check{s}_i^r, \quad z > z_b, \tag{21}$$

respectively, and where $\hat{b}^r$ and $\check{b}^r$ are again wave vector coefficients representing the contributions to scattering of different modes. Substitution of (19), (20), (21) and (7) into (18)

allows one to relate the scattered wave coefficients to those of the incident wave as

$$\begin{aligned}\Delta u_n(z') &= \omega\Delta z \sum_{r=1}^{3}\sum_{s=1}^{3} \frac{\mathrm{i}\,\mathrm{e}^{\mathrm{i}\omega q^r z}\,\mathrm{e}^{-\mathrm{i}\omega q^s z}\hat{s}_i^r\hat{s}_j^s}{2\rho^0(v^r)^2 q^r} \\ &\quad\times(-q^r q^s(\Delta\widetilde{\mathbf{C}}_{33})_{ij} + p_\alpha q^s(\Delta\widetilde{\mathbf{C}}_{\alpha 3})_{ij} \\ &\quad + p_\alpha q^r(\Delta\widetilde{\mathbf{C}}_{3\alpha})_{ij} - p_\alpha p_\gamma(\Delta\widetilde{\mathbf{C}}_{\alpha\gamma})_{ij} + \Delta\rho\delta_{ij})\hat{a}^s\,\mathrm{e}^{-\mathrm{i}\omega q^r z'}\hat{s}_n^r \\ &= \Delta z \sum_{r=1}^{3}\sum_{s=1}^{3} t_{\mathrm{U}}^{rs}\hat{a}^s\,\mathrm{e}^{-\mathrm{i}\omega q^r z'}\hat{s}_n^r \\ &= \sum_{r=1}^{3} \hat{b}^r\,\mathrm{e}^{-\mathrm{i}\omega q^r z'}\hat{s}_n^r, \quad z' < z_a \end{aligned} \tag{22}$$

and

$$\begin{aligned}\Delta u_n(z') &= \omega\Delta z \sum_{r=1}^{3}\sum_{s=1}^{3} \frac{\mathrm{i}\,\mathrm{e}^{-\mathrm{i}\omega q^r z}\,\mathrm{e}^{-\mathrm{i}\omega q^s z}\check{s}_i^r\check{s}_j^s}{2\rho^0(v^r)^2 q^r} \\ &\quad\times(q^r q^s(\Delta\widetilde{\mathbf{C}}_{33})_{ij} + p_\alpha q^s(\Delta\widetilde{\mathbf{C}}_{\alpha 3})_{ij} \\ &\quad - p_\alpha q^r(\Delta\widetilde{\mathbf{C}}_{3\alpha})_{ij} - p_\alpha p_\gamma(\Delta\widetilde{\mathbf{C}}_{\alpha\gamma})_{ij} + \Delta\rho\delta_{ij})\hat{a}^s\,\mathrm{e}^{\mathrm{i}\omega q^r z'}\check{s}_n^r \\ &= \Delta z \sum_{r=1}^{3}\sum_{s=1}^{3} r_{\mathrm{U}}^{rs}\hat{a}^s\,\mathrm{e}^{\mathrm{i}\omega q^r z'}\check{s}_n^r \\ &= \sum_{r=1}^{3} \check{b}^r\,\mathrm{e}^{\mathrm{i}\omega q^r z'}\check{s}_n^r, \quad z' > z_b\,. \end{aligned} \tag{23}$$

The quantity $r_{\mathrm{U}}^{rs}\Delta z$ (or $\mathbf{r}_{\mathrm{U}}\Delta z$ in matrix form) can be identified with the upward reflection matrix (e.g. Kennett 1983) for the slab, whereas $\mathbf{t}_{\mathrm{U}}\Delta z + \mathbf{I}$ corresponds to the transmission matrix for upward incidence. The corresponding matrices $\mathbf{r}_{\mathrm{D}}$, $\mathbf{t}_{\mathrm{D}}$ for a downward-propagating incident wave given by

$$u_i^0 = \sum_{r=1}^{3} \check{a}^r\,\mathrm{e}^{\mathrm{i}\omega q^r z}\check{s}_i^r \tag{24}$$

are

$$\begin{aligned} r_{\mathrm{D}}^{rs} &= \frac{\mathrm{i}\omega\,\mathrm{e}^{\mathrm{i}\omega q^r z}\,\mathrm{e}^{\mathrm{i}\omega q^s z}\hat{s}_i^r\check{s}_j^s}{2\rho^0(v^r)^2 q^r}\,(q^r q^s(\Delta\widetilde{\mathbf{C}}_{33})_{ij} - p_\alpha q^s(\Delta\widetilde{\mathbf{C}}_{\alpha 3})_{ij} \\ &\quad + p_\alpha q^r(\Delta\widetilde{\mathbf{C}}_{3\alpha})_{ij} - p_\alpha p_\gamma(\Delta\widetilde{\mathbf{C}}_{\alpha\gamma})_{ij} + \Delta\rho\delta_{ij}) \end{aligned} \tag{25}$$

and

$$\begin{aligned} t_{\mathrm{D}}^{rs} &= \frac{\mathrm{i}\omega\,\mathrm{e}^{-\mathrm{i}\omega q^r z}\,\mathrm{e}^{\mathrm{i}\omega q^s z}\check{s}_i^r\check{s}_j^s}{2\rho^0(v^r)^2 q^r}\,(-q^r q^s(\Delta\widetilde{\mathbf{C}}_{33})_{ij} - p_\alpha q^s(\Delta\widetilde{\mathbf{C}}_{\alpha 3})_{ij} \\ &\quad - p_\alpha q^r(\Delta\widetilde{\mathbf{C}}_{3\alpha})_{ij} - p_\alpha p_\gamma(\Delta\widetilde{\mathbf{C}}_{\alpha\gamma})_{ij} + \Delta\rho\delta_{ij})\,. \end{aligned} \tag{26}$$

The quantities $\mathbf{r}_{\mathrm{U}}$, $\mathbf{r}_{\mathrm{D}}$, $\mathbf{t}_{\mathrm{U}}$, $\mathbf{t}_{\mathrm{D}}$ may be used to assemble the reflection and transmission (R/T) response of an extended zone of arbitrary, 1-D heterogeneity using the method of invariant embedding (e.g. Bellman & Vasudevan 1986). In so doing, we consider a family of models with R/T matrices whose general properties remain invariant under the generation of the family. This invariance then provides a construct for advancing from the known R/T response of a simple model to the desired response of a more complex configuration. To illustrate this we consider the effect of welding a thin slab of material to the bottom of a region of heterogeneity with known R/T properties that extends from $z=0$ to some point $z=\zeta$ (see Fig. 2). The R/T properties of the region are referenced to levels $z=0$ and $z=Z$, and we may view this configuration as intermediate to one which comprises the desired vertical heterogeneity through the entire interval $[0, Z]$. The change in response due to the addition of the slab may be calculated through application of the addition rules for R/T matrices [Kennett 1983, eqs (6.3) and (6.4)] using the matrix quantities identified above for the thin slab. Consideration of the limit as $\Delta z \to 0$ leads to a system of Ricatti equations describing the evolution of the total R/T response:

$$\begin{aligned} \frac{\mathrm{d}\mathbf{R}_{\mathrm{U}}}{\mathrm{d}z} &= \mathbf{r}_{\mathrm{U}} + \mathbf{t}_{\mathrm{D}}\mathbf{R}_{\mathrm{U}} + \mathbf{R}_{\mathrm{U}}\mathbf{t}_{\mathrm{U}} + \mathbf{R}_{\mathrm{U}}\mathbf{r}_{\mathrm{D}}\mathbf{R}_{\mathrm{U}}\,, \\ \frac{\mathrm{d}\mathbf{T}_{\mathrm{U}}}{\mathrm{d}z} &= \mathbf{T}_{\mathrm{U}}\mathbf{t}_{\mathrm{U}} + \mathbf{T}_{\mathrm{U}}\mathbf{r}_{\mathrm{D}}\mathbf{R}_{\mathrm{U}}\,, \\ \frac{\mathrm{d}\mathbf{T}_{\mathrm{D}}}{\mathrm{d}z} &= \mathbf{t}_{\mathrm{D}}\mathbf{T}_{\mathrm{D}} + \mathbf{R}_{\mathrm{U}}\mathbf{r}_{\mathrm{D}}\mathbf{T}_{\mathrm{D}}\,, \\ \frac{\mathrm{d}\mathbf{R}_{\mathrm{D}}}{\mathrm{d}z} &= \mathbf{T}_{\mathrm{U}}\mathbf{r}_{\mathrm{D}}\mathbf{T}_{\mathrm{D}}\,. \end{aligned} \tag{27}$$

This is an initial value problem which must be supplemented with initial conditions. Clearly, at $z=0$ there is no heterogeneity and so no reflected wavefield, i.e. $\mathbf{R}_{\mathrm{U}}(0)=\mathbf{R}_{\mathrm{D}}(0)=\mathbf{0}$. The transmitted wavefield is not zero, however, nor is it in general the identity matrix, since there will be some phase income between $z=0$ and $z=Z$ for the incident wavefield. The Ricatti equations must account for the effect of heterogeneity through a phase correction to the incident wave, as is readily evident upon inspection of the trivial case $\Delta c_{ijkl}(z)=\Delta\rho(z)=0$ on the interval $[0, Z]$. Thus, the initial conditions on transmission must be $\mathbf{T}_{\mathrm{U}}(0)=\mathbf{T}_{\mathrm{D}}(0)=\mathrm{diag}(\mathrm{e}^{\mathrm{i}\omega q^r Z})$ if the phase behaviour of the system is to be properly described.

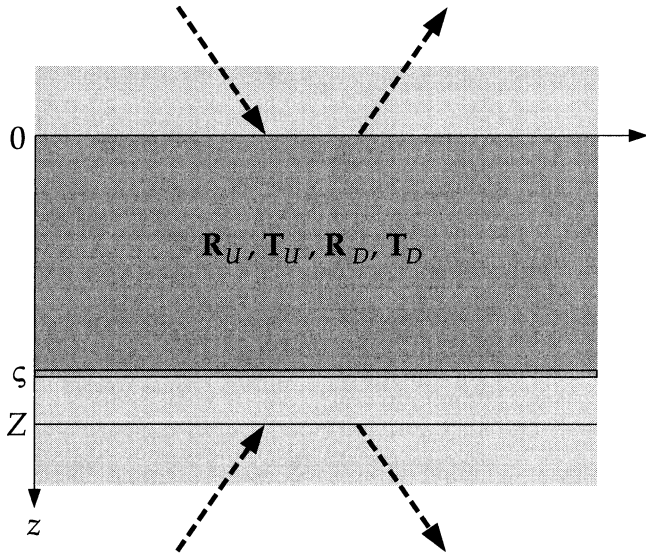


**Figure 2.** Derivation of the matrix Ricatti equations (22), (23), (25) and (26) proceeds by evaluating the change in response due to the welding of a vanishingly thin slab of material at the base of a zone with known $\mathbf{R}_{\mathrm{U}}$, $\mathbf{T}_{\mathrm{U}}$, $\mathbf{R}_{\mathrm{D}}$, $\mathbf{T}_{\mathrm{D}}$.

Solution of the non-linear system of ordinary differential equations in (27) yields the exact R/T matrices for a zone of arbitrary vertical heterogeneity and as such these may be manipulated and incorporated within the framework of R/T algebra formulated by Kennett (1983). In particular, one may readily alternate between different reference or embedding media (including anisotropy) above and/or below the heterogeneity through the welding of half-spaces using, again, the R/T addition rules but now for incorporation of interfaces.

It is also worth emphasizing that the formulation described here may be used to infer the properties of the wavefield within the heterogeneous zone. This is accomplished by considering the internal wavefield in terms of forward- and backward-propagating waves in the reference medium with coefficient vectors that vary with $z$, i.e.

$$u_i = \sum_{r=1}^{3} \check{a}^r(z)\, \mathrm{e}^{\mathrm{i}\omega q^r z} \check{s}_i^r + \hat{a}^r(z)\, \mathrm{e}^{-\mathrm{i}\omega q^r z} \hat{s}_i^r, \quad 0 < z < Z, \tag{28}$$

where the depth dependence of the wave coefficients has been explicitly identified. Under this interpretation, the coefficients of the wavefield are easily shown to satisfy

$$\frac{\mathrm{d}}{\mathrm{d}z}\begin{pmatrix} \check{\mathbf{a}} \\ \hat{\mathbf{a}} \end{pmatrix} = \begin{pmatrix} \mathbf{t}_\mathrm{D} & \mathbf{r}_\mathrm{U} \\ -\mathbf{r}_\mathrm{D} & -\mathbf{t}_\mathrm{U} \end{pmatrix} \begin{pmatrix} \check{\mathbf{a}} \\ \hat{\mathbf{a}} \end{pmatrix} \tag{29}$$

(*cf*. Kennett 1984; Bellman & Vasudevan 1986). This is a boundary value problem which, when posed in terms of a band of heterogeneity on $[0, Z]$, has boundary conditions where either $\check{\mathbf{a}}(0)$ is prescribed and $\hat{\mathbf{a}}(Z) = 0$ (corresponding to downward incidence) or $\hat{\mathbf{a}}(Z)$ is prescribed and $\check{\mathbf{a}}(0) = 0$ (upward incidence). As noted by Kennett (1984), the boundary value problem is more difficult to solve numerically than the initial value problem in (27) and it is preferable, therefore, to work within the R/T formulation to extract the behaviour of $\check{\mathbf{a}}(z)$, $\hat{\mathbf{a}}(z)$.

Consider then the wavefield at some level $z = \zeta$ within the heterogeneity, that is $0 < \zeta < Z$, resulting from a wave incident upon the heterogeneous zone from above. The downgoing wavefield at this level is the sum of the transmitted waves from $z = 0$ and downward-propagating reflected waves at $z = \zeta$. Therefore, we may write

$$\check{\mathbf{a}}(\zeta) = \mathbf{T}_\mathrm{D}(\zeta)\check{\mathbf{a}}(0) + \mathbf{R}_\mathrm{U}(\zeta)\hat{\mathbf{a}}(\zeta), \tag{30}$$

and, following a similar line of argument,

$$\hat{\mathbf{a}}(0) = \mathbf{T}_\mathrm{U}(\zeta)\hat{\mathbf{a}}(\zeta) + \mathbf{R}_\mathrm{D}(\zeta)\check{\mathbf{a}}(0) = \mathbf{R}_\mathrm{D}(Z)\check{\mathbf{a}}(0). \tag{31}$$

The quantity $\check{\mathbf{a}}(0)$ is prescribed and the R/T matrices $\mathbf{R}_\mathrm{U}(\zeta)$, $\mathbf{R}_\mathrm{D}(\zeta)$, $\mathbf{T}_\mathrm{U}(\zeta)$, $\mathbf{T}_\mathrm{D}(\zeta)$ for all desired subintervals $[0, \zeta]$ of the heterogeneous band $[0, Z]$ can be stored during a single integration of (27) for $\mathbf{R}_\mathrm{U}(Z)$, $\mathbf{R}_\mathrm{D}(Z)$, $\mathbf{T}_\mathrm{U}(Z)$, $\mathbf{T}_\mathrm{D}(Z)$ at no additional computational expense (note that trivial phase adjustments must be applied to $\mathbf{R}_\mathrm{U}$, $\mathbf{T}_\mathrm{U}$, $\mathbf{T}_\mathrm{D}$ to account for the change in reference level from $Z$ to $\zeta$). Thus, the only unknowns are the internal wavefield coefficients, which are solved for as

$$\hat{\mathbf{a}}(\zeta) = \mathbf{T}_\mathrm{U}^{-1}(\zeta)(\mathbf{R}_\mathrm{D}(Z) - \mathbf{R}_\mathrm{D}(\zeta))\check{\mathbf{a}}(0) \tag{32}$$

and

$$\check{\mathbf{a}}(\zeta) = (\mathbf{T}_\mathrm{D}(\zeta) + \mathbf{R}_\mathrm{U}(\zeta)\mathbf{T}_\mathrm{U}^{-1}(\zeta)(\mathbf{R}_\mathrm{D}(Z) - \mathbf{R}_\mathrm{D}(\zeta)))\check{\mathbf{a}}(0). \tag{33}$$

For upward incidence where $\hat{\mathbf{a}}(Z)$ is prescribed, analogous arguments lead to

$$\check{\mathbf{a}}(\zeta) = \mathbf{T}_\mathrm{U}^{-1}(\zeta)\mathbf{T}_\mathrm{U}(Z)\hat{\mathbf{a}}(Z) \tag{34}$$

and

$$\hat{\mathbf{a}}(\zeta) = \mathbf{R}_\mathrm{U}(\zeta)\mathbf{T}_\mathrm{U}^{-1}(\zeta)\mathbf{T}_\mathrm{U}(Z)\hat{\mathbf{a}}(Z). \tag{35}$$

Lastly, it should be noted that the wavefield decomposition presented here is not unique (see e.g. Sluijter 1970). Ursin (1983) solves the 1-D vertical heterogeneity problem using the Ricatti equations in (27) referenced to a continuum of local modes (rather than a single reference mode set as is done here), where the local mode set at level $z$ is defined by the three elastic wave modes that would propagate in a homogeneous medium with the same material properties as at $z$. In that case, the coefficient matrices $\mathbf{r}_\mathrm{U}$, $\mathbf{r}_\mathrm{D}$, $\mathbf{t}_\mathrm{U}$, $\mathbf{t}_\mathrm{D}$ are constructed from products of inverse eigenvector matrices and vertical derivatives of eigenvector matrices, as opposed to terms involving material property perturbations in (22), (23), (25) and (26). Moreover, the initial conditions on transmission matrices for the local mode construction are properly given by $\mathbf{T}_\mathrm{U}(0) = \mathbf{T}_\mathrm{D}(0) = \mathbf{I}$.

## EXAMPLE 1: A UNIFORM ANISOTROPIC LAYER

Our first model comprises a 15 km thick uniform layer with the elastic properties of quasi-monoclinic anorthite (as defined by Babuska & Cara 1991) embedded within an isotropic reference medium with $P$ velocity 8000 m s$^{-1}$, $S$ velocity 5000 m s$^{-1}$ and density 4000 kg m$^{-3}$. Anorthite is characterized by $P$- and $S$-wave anisotropies of 36 and 52 per cent (Anderson 1989), average $P$- and $S$-wave velocities of 6428 and 3526 m s$^{-1}$, and a density of 2640 kg m$^{-3}$. Since the model comprises homogeneous layers, the R/T response can be simply calculated using standard reflectivity techniques (Kennett 1983; Martin & Thomson 1998) as well as the invariant embedding approach just described, thereby permitting a convenient numerical check (note that the standard reflectivity approach is clearly computationally superior for models comprising homogeneous layers, but this advantage and formal exactitude are lost for more general 1-D structures).

The ordinary differential equations in (27) were solved using a predictor–corrector (Adams–Moulton) method, which is relatively efficient for the somewhat complicated functional forms in (22), (23), (25) and (26). Fig. 3 shows selected elements from R/T matrices computed using reflectivity, the present formulation, and for invariant embedding but using the conventional (as opposed to thin-scatterer) Born approximation, for a horizontal slowness $p_x = p_y = 0.10$ s km$^{-1}$ and a number of frequencies. This choice of $p_\alpha$ results in $P$-wave evanescence within the anorthite layer. The solutions from reflectivity and eqs (27) shown in Figs 3(a) and (b) are equivalent to any specified tolerance in the numerical integration, whilst a clear disparity exists with the results using the conventional Born approximation. This is not surprising given velocity contrasts exceeding 20 per cent between the reference medium and heterogeneity. Determination of R/T matrices in evanescent regimes using (27) appears, on the basis of a limited number of numerical experiments, to be quite stable, as might be expected given the general R/T formulation (Kennett 1983) and stability

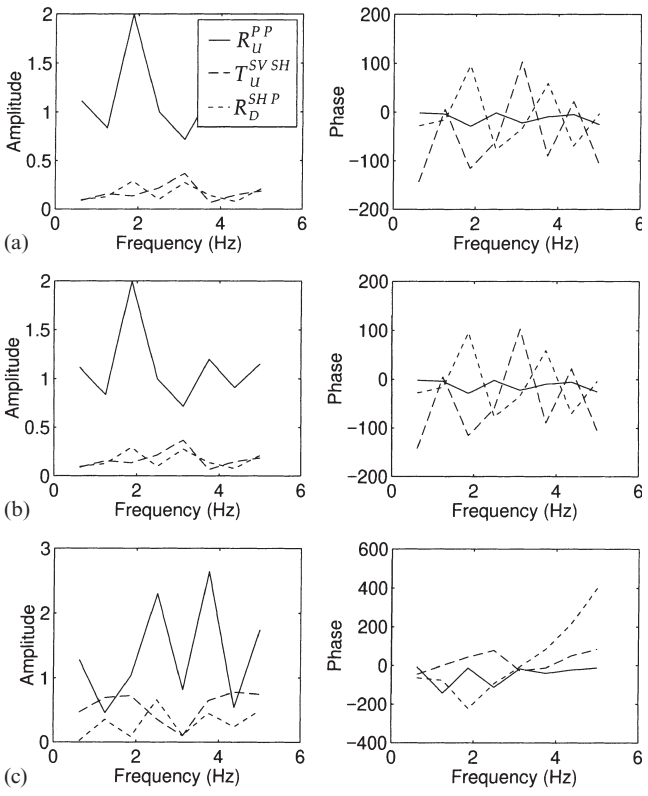


**Figure 3.** Selected elements of the R/T response for a 10 km thick layer of quasi-monoclinic anorthite (Babuska & Cara 1991) embedded within an isotropic medium at a number of frequencies. Responses calculated using (a) reflectivity (Martin & Thomson 1998), (b) invariant embedding with the thin-scatterer Born approximation and (c) invariant embedding with the conventional Born approximation. See text for model details.

characteristics of the Ricatti transformations (Bellman & Vasudevan 1986).

## EXAMPLE 2: *Ps* CONVERSION FROM AN ISOTROPIC VELOCITY GRADIENT

Richards (1972) examined the reflection characteristics of a gradient zone sandwiched between two uniform media using asymptotic methods in order to place constraints on the transition width of the 660 km discontinuity as determined from the underside reflected phase $P'P'$. We are interested in the related problem for $P \rightarrow S$ mode conversions and, specifically, in the scaling between gradient transition interval and wavelength required to produce strong scattered phases. For comparison purposes, we consider, the same isotropic velocity model $V_p(660^-) = 10.0$ km s$^{-1}$, $V_p(660^+) = 10.95$ km s$^{-1}$, $V_s(660^-) = 5.0$ km s$^{-1}$, $V_s(660^+) = 5.75$ km s$^{-1}$, $\rho(660^-) = 4130$ kg m$^{-3}$, $\rho(660^+) = 4340$ kg m$^{-3}$, and horizontal slowness $p_1 = 0.0252$ s km$^{-1}$. Results are shown in Fig. 4 and agree with those of Richards (1972) for intramode $P$ reflection. In particular, $R_{\mathrm{D}}^{PP}$ (first and second superscripts denote scattered and incident modes, respectively) is seen to decay rapidly as the transition interval increases, and is approximately 50 per cent of its maximum value at a transition thickness $\Delta z = \lambda/4$. A similar relation is observed for the $SH$ and $SV$ modes and for the diagonal components of $\mathbf{R}_{\mathrm{U}}$, whilst reflected conversions exhibit decay rates that are intermediate between those for intramode $P$- and $S$-wave reflections. Transmitted conversions, shown in Fig. 4(d), are noticeably less sensitive to transition width, with the first minimum in the transmission response occurring at roughly twice the transition width for that characterizing $P \rightarrow P$ reflections.

This behaviour is evidently governed by the sum of the (signed) vertical slownesses characterizing the relevant mode

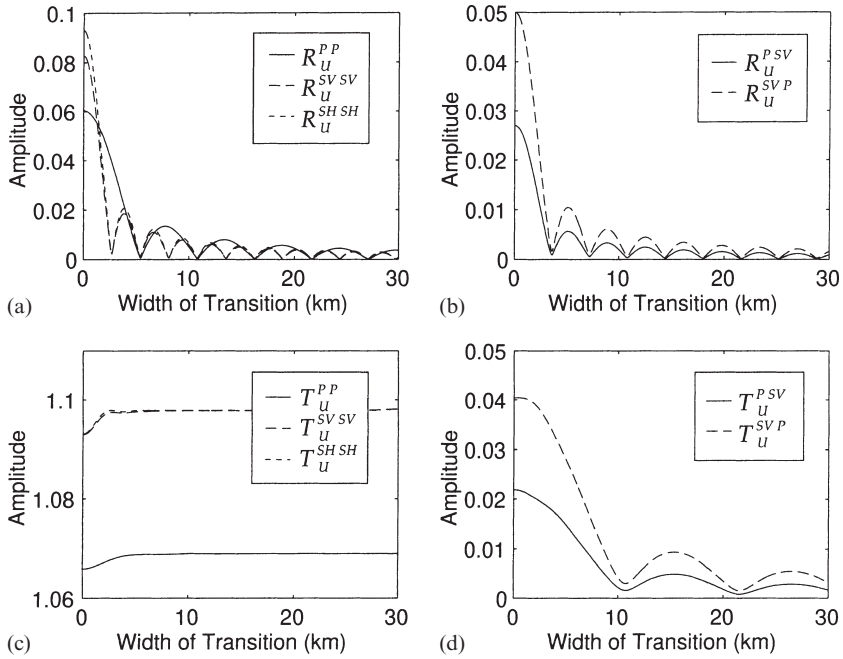


**Figure 4.** The absolute R/T response for an (isotropic) model of the 660 km discontinuity examined previously by Richards (1972) as a function of gradient transition width. Selected elements are shown for (a) reflection coefficients, (b) reflection conversion coefficients, (c) transmission coefficients and (d) transmission conversion coefficients, all for upward incidence.

interactions as present in (22), (23), (25) and (26). Intramode transmission responses (that is, the diagonal elements of $\mathbf{T}_D$, $\mathbf{T}_U$) do not exhibit an oscillatory behaviour since the vertical slownesses cancel in those cases. Accordingly, the partial cancellation of vertical slowness in the mode conversion case leads to transmission responses that are less sensitive in general than reflections to gradients. Thus, if $\Delta z = \lambda/4$ is considered an appropriate rule of thumb for intramode reflections at near-vertical incidence, the corresponding relation for intramode conversions is $\Delta z = \lambda_P/2$, where $\lambda_P$ is the wavelength of the compressional mode.

## EXAMPLE 3: MANTLE *Ps* CONVERSIONS AT YELLOWKNIFE

This study was motivated in large part by observations of teleseismic *P*-wave data recorded at broad-band stations of the Yellowknife array (YKA) in Canada's Northwest Territories (Bostock 1998). The location of YKA with respect to global seismicity and over 10 years of archived data allows a detailed examination of the *P*-wave impulse response (or 'receiver function') as a function of ray parameter and backazimuth. Fig. 5 shows a grey-shade plot of the radial and transverse

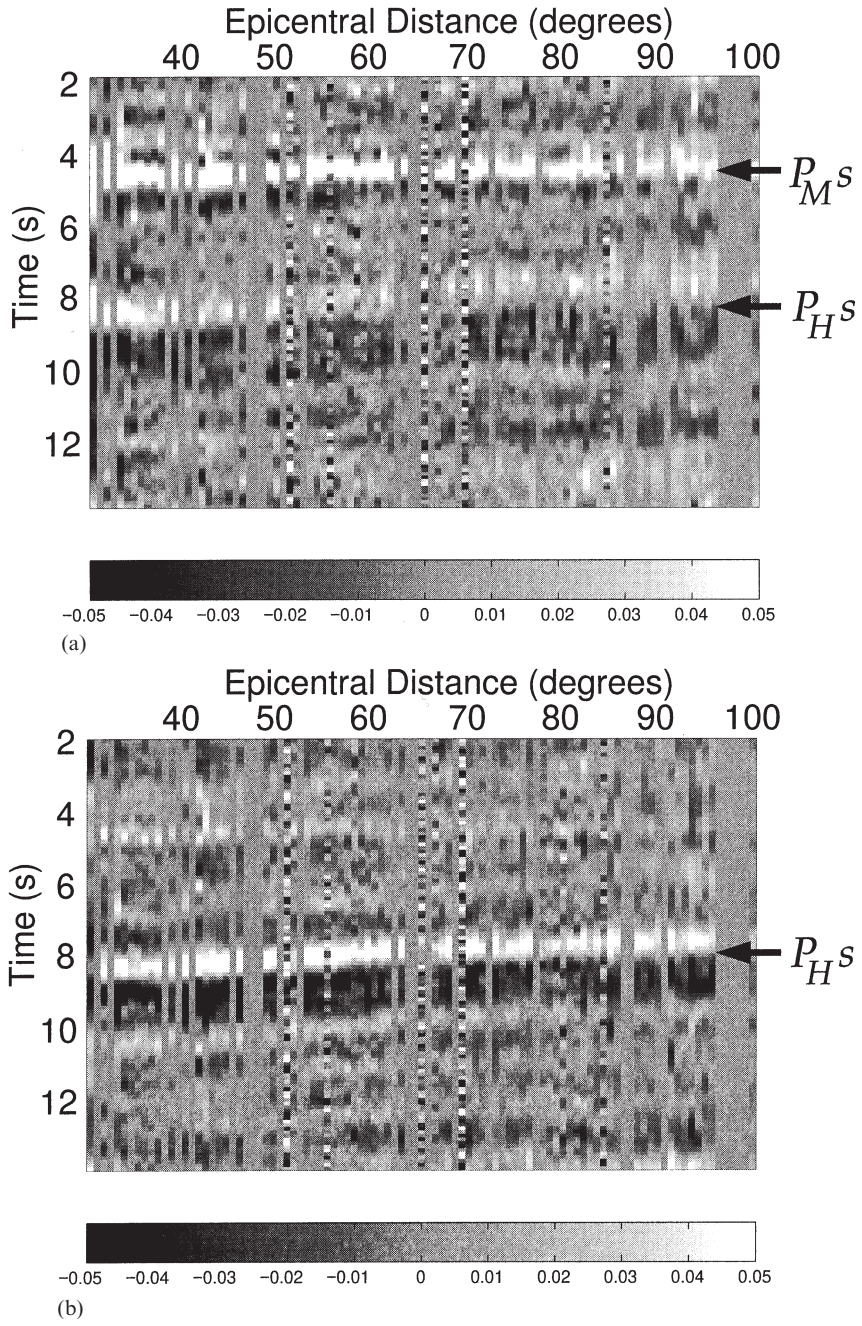


**Figure 5.** Broad-band (0.02–5.0 Hz) *P*-wave impulse response at YKA for backazimuthal corridor N275°W–N312°W as a function of time and epicentral distance. (a) Radial component shows clear conversions from the Moho ($P_Ms$) at ~4.5 s and a deeper mantle layer ($P_Hs$) near 8–9 s. (b) Transverse component is dominated by $P_Hs$.

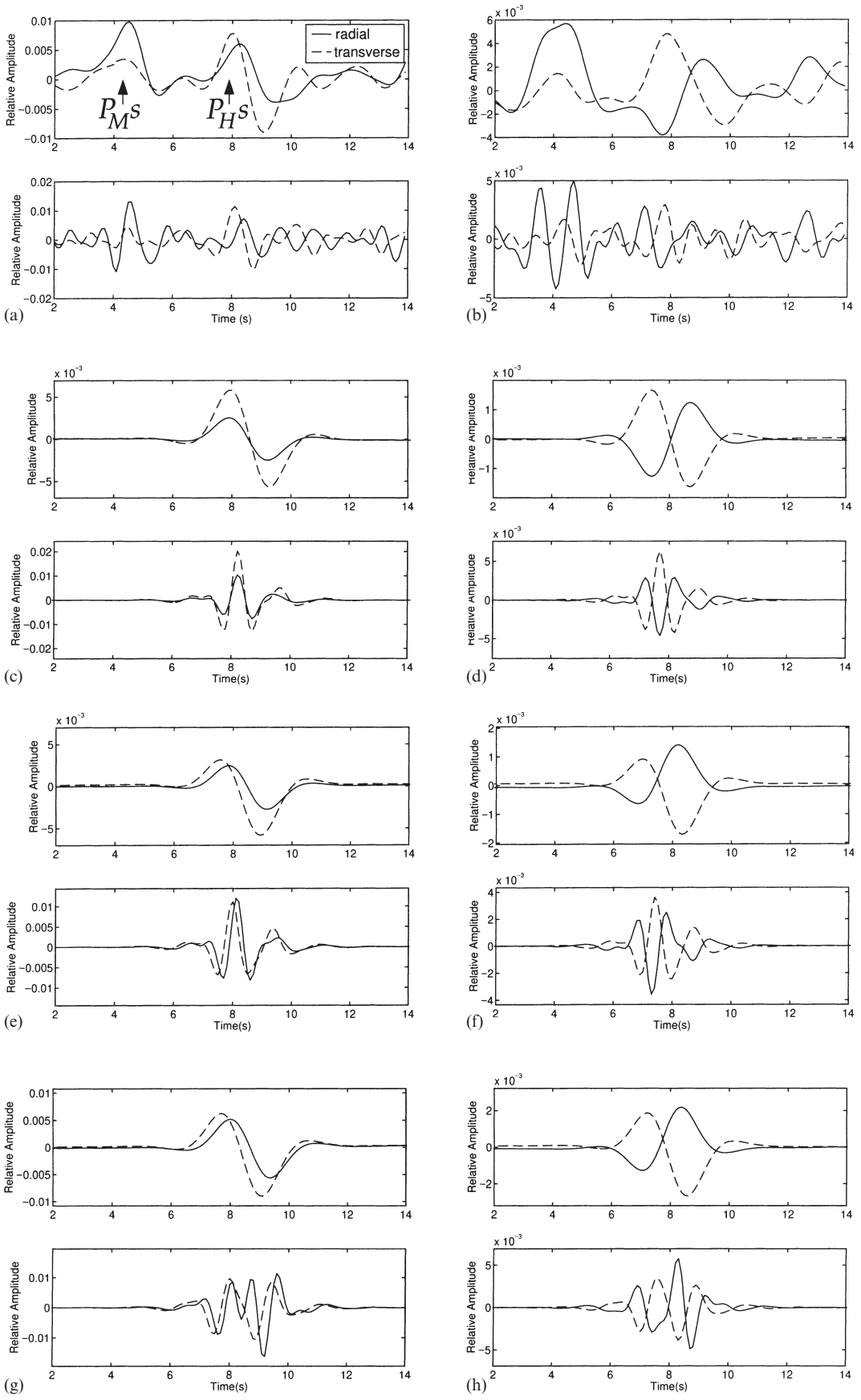


**Figure 6.** Impulse response functions at YKA from (a) N298°E backazimuth, 45° epicentral distance and (b) N04°E backazimuth, 84° epicentral distance. Upper and lower panels in both (a) and (b) have been filtered at 0.02–0.5 Hz and 0.5–5.0 Hz, respectively. (c), (d) Corresponding synthetic responses for $P_{\mathrm{H}}s$ determined for a 10 km thick anisotropic gradient zone embedded within an isotropic reference medium. (e), (f) Corresponding synthetic responses for $P_{\mathrm{H}}s$ determined for a 10 km thick anisotropic gradient zone overlain by a mildly anisotropic cap. (g), (h) Corresponding synthetic responses for $P_{\mathrm{H}}s$ determined for a 10 km thick uniform anisotropic layer overlain by a mildly anisotropic cap. See text for model details.

impulse responses between 2 and 14 s for a narrow back-azimuthal window (275°–312°) as a function of epicentral distance. These data correspond to earthquakes occuring along the western Pacific subduction zones. A white streak on the radial component near 5 s corresponds to the *P* to *S* conversion from the Moho, $P_{M}s$, originating near 36 km depth. Following this at $\sim$ 8–9 s on both radial and transverse components is a two-toned arrival, $P_{H}s$, which has been previously interpreted as originating from a 10 km thick anisotropic layer near 75 km depth. These plots represent a broad-band response (0.02–5.0 Hz) and it is apparent that the second (negative polarity) lobe exhibits a somewhat lower frequency content than the first. To investigate this in more detail, we plot a sample impulse response corresponding to $\sim 45^{\circ}$ distance ($p = 0.0716$ s km$^{-1}$), 298° backazimuth and filtered to high-pass (0.5–5.0 Hz) and low-pass (0.02–0.5 Hz) bands for both components in Fig. 6(a). The low-pass response clearly shows the double-lobed character evident in Fig. 5, whereas the high-pass response appears to exhibit strong peaks associated only with the upper boundary arrival. The extinction of the second lobe occurs at frequencies higher than $\sim 0.5$ Hz. Also apparent in Fig. 6(a) is a slight shift between the radial and transverse signals of $\sim 0.4$ s. A similar plot is shown in Fig. 6(b) for an epicentral distance of $\sim 84^{\circ}$ ($p = 0.0457$ s km$^{-1}$) and back-azimuth N04°E. The change in backazimuth has produced a polarity reversal of $P_{H}s$ on the radial component which signals the presence of some component of azimuthal anisotropy.

The frequency dependence of the second lobe of $P_{H}s$ suggests that the lower boundary of the anisotropic layer is a transition. Guided by the observations made in the previous section, we consider a revised model which comprises a 10 km thick zone of heterogeneity embedded within an isotropic medium with $V_p = 8.0$ km s$^{-1}$, $V_s = 4.5$ km s$^{-1}$, $\rho = 3.3$ kg m$^{-3}$. The heterogeneity is a gradient zone of azimuthal anisotropy which increases linearly from zero at the base of the zone to $\delta V_p / V_p = 0.1$, $\delta V_s / V_s = 0.05$ at a discontinuous upper boundary. Here we have used the model parametrization suggested by Farra *et al.* (1991) with $\eta = F/(A - 2L) = 1.03$. Synthetic seismograms for a geometrical configuration corresponding approximately to the data in Figs 6(a) and (b) are shown in Figs 6(c) and (d). These show the same style of frequency dependence as the data; in particular, the low-pass seismograms show 'dipolar' (positive and negative) lobes, whilst strong conversions at higher frequencies are restricted to signal from the upper boundary. The synthetics fail, however, to capture the slight $\sim 0.4$ s phase delay between radial and transverse components present in the data. Evidently, anisotropy within the 10 km thick heterogeneous zone is insufficient to promote significant splitting of shear modes. It is not difficult, however, to achieve reasonable agreement with the data, as shown in Figs 6(e) and (f), by introducing a mildly anisotropic perturbation ($\delta V_p / V_p = 0.03$, $\delta V_s / V_s = 0.01$, $\eta = 1.03$, orientation as before) to the 75 km interval above the gradient zone. The final series of seismograms is plotted in Figs 6(g) and (h) for comparative purposes, and represents a model where the heterogeneous zone is now a 10 km thick uniform anisotropic layer ($\delta V_p / V_p = 0.10$, $\delta V_s / V_s = 0.05$, $\eta = 1.03$, orientation as before) bounded above by the same 75 km mildly anisotropic cap. Although similar to the seismograms in Figs 6(e) and (f) at low frequencies, the response to the uniform layer at short periods clearly shows the effect of the conversion at the lower boundary.

## CONCLUSIONS

We have extended the results of previous studies and shown how exact R/T matrices for arbitrary 1-D, anisotropic stratification may be constructed from material property perturbations using the technique of invariant embedding. An essential ingredient in this construction is a form of Born approximation appropriate for thin scatterers exhibiting arbitrary departures in physical properties from the embedding reference medium. The formulation allows for efficient computation of the wavefield internal to the heterogeneity using R/T matrices for the heterogeneity and portions thereof.

Application of the theory to mode conversion of plane waves from velocity gradients indicates that transmission conversions are less sensitive to this form of heterogeneity than reflections. Conversions of significant amplitude occur where the gradient transition interval is less than $\lambda_P/2$ (versus $\lambda_P/4$ for *P* reflections; Richards 1972). We have applied this observation and the R/T theory to model teleseismic *P* coda recorded at YKA. The primary objective of this exercise has been to isolate those processes which appear to have exerted a controlling influence on the phase behaviour of $P_{H}s$. We conclude that a layer structure comprising a transition zone approximately 10 km in thickness with anisotropy increasing to an abrupt upper boundary is capable of explaining the essential characteristics exhibited by these mantle mode conversions. The result has important geodynamic implications; specifically, it is consistent with an interpretation that the upper boundary of the heterogeneity represents an ancient thrust fault along which a shallowly subducting former oceanic plate has been juxtaposed against overriding lithosphere (Bostock 1998). Under this interpretation, the anisotropic gradient zone is associated with a strain field generated during subduction that diminishes with depth from the contact and which coincides closely with the depth extent formerly occupied by oceanic crust. A more comprehensive, quantitative analysis of the entire lithospheric column below YKA will be the subject of a future study.

## ACKNOWLEDGMENTS

I am grateful to Bob Odom, Colin Thomson and Brian Kennett for fruitful discussions on various aspects of this work and to Wolfgang Friederich and an anonymous reviewer for helpful comments. Yellowknife Array data were graciously provided by the Geological Survey of Canada. Financial support for this work was provided through Natural Sciences and Engineering Research Council of Canada (NSERC) research grant OGP0138004.

## REFERENCES

Anderson, D.L., 1989. *Theory of the Earth,* Blackwell Scientific Publications, London.

Babuska, V. & Cara, M., 1991. *Seismic Anisotropy in the Earth,* Kluwer Academic, Dordrecht.

Backus, G.E., 1962. Long-wave elastic anisotropy produced by horizontal layering, *J. geophys. Res.,* **67,** 4427–4440.

Bellman, R. & Vasudevan, R., 1986. *Wave Propagation, an Invariant Imbedding Approach,* D. Riedel, Dordrecht.

Benz, H.M. & Vidale, J.E., 1993. Sharpness of upper-mantle discontinuities determined from high-frequency reflections, *Nature,* **365,** 147–150.

Bostock, M.G., 1998. Mantle stratigraphy and evolution of the Slave province, *J. geophys. Res.,* **103,** 21 183–21 200.

Chapman, C.H., 1974. The turning point of elastodynamic waves, *Geophys. J. R. astr. Soc.,* **39,** 613–621.

Farra, V., Vinnik, L.P., Romanowicz, B., Kosarev, G.L. & Kind, R., 1991. Inversion of teleseismic *S* particle motion for azimuthal anisotropy in the upper mantle: a feasibility study, *Geophys. J. Int.,* **106,** 421–431.

Grand, S.P., 1994. Mantle shear structure beneath the Americas and surrounding oceans, *J. geophys. Res.,* **99,** 11 591–11 621.

Herrera, I. & Mal, A.K. 1965., A perturbation method for elastic wave propagation, II—small inhomogeneities, *J. geophys. Res.,* **70,** 871–883.

Hudson, J.A., 1977. Scattered waves in the coda of *P*, *J. Geophys.,* **43,** 359–374.

Kennett, B.L.N., 1983. *Seismic Wave Propagation in Stratified Media,* Cambridge University Press, Cambridge.

Kennett, B.L.N., 1984. Guided wave propagation in laterally varying media—I. Theoretical development, *Geophys. J. R. astr. Soc.,* **79,** 235–255.

Kennett, B.L.N. & Illingworth, M.R., 1981. Seismic waves in a stratified half space—III. Piecewise smooth models, *Geophys. J. R. astr. Soc.,* **66,** 633–675.

Martin, B.E. & Thomson, C.J., 1998. Modelling surface waves in anisotropic structures, II, Examples, *Phys. Earth planet. Inter.,* **103,** 253–279.

McCoy, J. & Frazer, L.N., 1986. Propagation modelling based on wavefield factorization and invariant imbedding, *Geophys. J. R. astr. Soc.,* **86,** 703–717.

Petersen, N., Vinnik, L., Kosarev, G., Kind, R., Oreshin, S. & Stammler, K., 1993. Sharpness of the mantle discontinuities, *Geophys. Res. Lett.,* **20,** 859–862.

Richards, P.G., 1972. Seismic waves reflected from velocity gradient anomalies in Earth's upper mantle, *J. Geophys.,* **38,** 517–527.

Richards, P.G. & Frasier, C.W., 1976. Scattering of elastic waves from depth-dependent inhomogeneities, *Geophysics,* **41,** 441–458.

Sluijter, F.W., 1970. Arbitrariness of dividing the total field in an optically inhomogeneous medium into direct and reversed waves, *J. Opt. Soc. Am.,* **60,** 8–10.

Tromp, J. & Snieder, R. 1989., The reflection and transmission of plane *P*- and *S*-waves by a continuously stratified band: a new approach using invariant imbedding, *Geophys. J.,* **96,** 447–456.

Ursin, B., 1983. Review of elastic and electromagnetic wave propagation in horizontally layered media, *Geophysics,* **48,** 1063–1081.

van der Hilst, R.V., Widiyantoro, S. & Engdahl, E.R., 1997. Evidence for deep mantle circulation from global tomography, *Nature,* **386,** 578–584.

Woodhouse, J.H., 1974. Surface waves in a laterally varying layered structure, *Geophys. J. R. astr. Soc.,* **37,** 461–490.

Woodhouse, J.H., 1978. Asymptotic results for elastodynamic propagator matrices in plane stratified and spherically stratified earth models, *Geophys. J. R. astr. Soc.,* **54,** 263–280.